Multigrating phase conjugation: chaotic results

M. R. Belić and D. Timotijević

Institute of Physics, P.O. Box 57, 11001 Belgrade, Yugoslavia

W. Krolikowski

Electro-Optics Technology Center, Tufts University, Medford, Massachusetts 02155

Received September 14, 1990; revised manuscript received January 8, 1991

Slowly varying envelope wave equations describing degenerate four-wave mixing (4WM) in photorefractive phase-conjugate mirrors are solved exactly, in terms of quadratures. Multigrating 4WM geometry is assumed, with the transmission and reflection gratings contributing equally and with the counterpropagating pump–pump interaction accounted for. The original boundary-value problem is transformed into an initial-value problem, which is treated by an iteration procedure. It is shown that within the iterative boundary-fitting procedure the multistability of solutions takes place and that the intensity reflectivity of the mirror may become chaotic. The strange attractor thus arising is analyzed with the use of standard methods of nonlinear dynamics.

1. INTRODUCTION

Owing to the great potential applicability of optical phase conjugation (OPC), instabilities arising in phase-conjugating systems have attracted considerable attention recently.[1] The interest in such systems stems from the fact that they effectively achieve time reversal of a propagating wave front, with rich possibilities of lensless autocorrection in various optical instruments.[2] However, being by its nature a high-gain self-oscillating process, the generation of phase conjugate wave fronts is also prone to instabilities.[3–6]

Chaos in OPC thus far has been displayed in two kinds of experimental arrangement: resonator geometries[4] and single photorefractive crystals.[5,6] While the occurrence of chaos in resonator geometries should present no surprise, the origins of chaos in single crystals is not yet fully understood. Instabilities in such systems often follow from a boundary-value analysis of steady-state equations and should be handled with caution. It may sound surprising, but numerical instabilities may follow the same routes to chaos as those taken by the underlying models.

Resonators, conjugate or not, represent textbook examples of systems apt to become chaotic. The ingredients necessary for chaos are readily available in such systems: nonlinearity is provided by the phase conjugate (PC) or any other active or passive medium, driving comes from the laser beams pumping the medium, and feedback is caused by the normal mirror enclosing the cavity. It would indeed present a surprise if such systems were not chaotic in some region of the parameter space.[7]

The situation with single crystals, or individual PC mirrors, is not so clear. Instabilities or chaos in single crystals with a standard four-wave mixing (4WM) geometry arise under different operational conditions or in different models of 4WM operation. One prominent model is given in Ref. 6, where it is suggested that multigrating operation of the PC mirror and multiple interaction regions are essential for the appearance of chaos. Another model is given by the present authors,[8] in which the crucial destabilizing element is an externally applied dc electric field. In both models operation above the self-oscillation threshold (i.e., strong enough coupling between the waves) is assumed, and an analysis of time-dependent equations is carried out.

In this paper we investigate stable solutions and instabilities arising in the single interaction region of a photorefractive crystal, assuming multigrating 4WM, no external electric field, and a steady state. Slowly varying envelope equations are solved with the use of a novel integration procedure, in which the equations are solved exactly in terms of quadratures, and the fitting of boundary values is achieved by an iteration procedure in the parameter space. The iterative mapping may become unstable in some regions of the parameter space, causing multiple solutions of wave equations and eventually chaotic reflectivity of the crystal.

It should be pointed out that in a procedure such as this one it is difficult to be certain that the generated instabilities have a physical meaning. One way to increase the level of confidence is to solve the problem (equations) by more than one method. If the instabilities persist, then they are more likely the property of the model itself and not of the numerics used. We performed such a check in our investigation, and we are certain that the instabilities indeed belong to the model. Nonetheless, the question of the physical reality of instabilities may still be raised. There might exist some additional physical criterion not contained in the model, which could preclude the development of instabilities. A question like this can be resolved only by experiment or by a more comprehensive theory.

The paper is organized in the following fashion. Section 2 discusses the method of integration and stable solutions. Section 3 deals with instabilities, and Section 4 presents a summary of our results.

0740-3224/91/081723-09$05.00

2. SOLUTION METHOD

We consider multigrating 4WM in photorefractive crystals in standard geometry and standard notation. Two counterpropagating pumps (A_1 and A_2) are shining on the crystal from the opposite sides, and a signal A_4 is incident upon the crystal from the side of the pump A_1. Photorefractive interaction of these waves in the crystal generates the PC replica A_3 of the signal. The process is described by a set of four wave equations for the slowly varying envelopes of the four components of the electric field oscillating at allowed k vectors and at the degenerate frequency. There are four ways in which the waves can mix and build diffraction gratings in the crystal. Two of these contribute to the PC wave generation and are commonly denoted the transmission and the reflection geometry, respectively.[9] The other two come from the two-wave mixing of the pumps and of the probe with the PC. We assume here that the transmission and reflection gratings contribute equally and that the two-wave interaction between the probe and the PC signal can be neglected. The rationale behind such an approximation is provided in Ref. 10. The relevant wave equations, deduced from their general form, as given in Ref. 9, are

$$IA_1' = g(A_T A_4 - A_R A_3) - \gamma|A_2|^2 A_1, \tag{1a}$$

$$IA_2^{*\prime} = g(A_T A_3^* - A_R A_4^*) - \gamma|A_1|^2 A_2^*, \tag{1b}$$

$$IA_3' = -g(A_T A_2 + A_R^* A_1), \tag{1c}$$

$$IA_4^{*\prime} = -g(A_T A_1^* + A_R^* A_2^*), \tag{1d}$$

where $I = \sum|A_i|^2$ is the total intensity, g and γ are the wave coupling coefficients (real numbers here), and $A_T = A_1A_4^* + A_2^*A_3$ and $A_R = A_1A_3^* + A_2^*A_4$ are the amplitudes of the transmission and reflection gratings, respectively. Our goal is to solve these equations accurately and rapidly as a boundary-value problem and, at the same time, to handle readily instabilities that may arise along the way. The method of solution is as follows.

First, when Eqs. (1) are rewritten in terms of intensities and phases, it is seen that the only phase variable to figure in the equations is the relative phase $\phi = \phi_4 + \phi_3 - \phi_2 - \phi_1$. Assuming exact phase conjugation (i.e., $\phi = 0$ or π, depending on the setup) eliminates the phase equation, and the remaining set of intensity equations becomes

$$II_1' = 2\gamma I_1 I_2 - 2gI_1(I_4 - I_3), \tag{2a}$$

$$II_2' = 2\gamma I_2 I_1 + 2gI_2(I_4 - I_3), \tag{2b}$$

$$II_3' = 2gI_3(I_1 + I_2) + 4g(I_1I_2I_3I_4)^{1/2}, \tag{2c}$$

$$II_4' = 2gI_4(I_1 + I_2) + 4g(I_1I_2I_3I_4)^{1/2}. \tag{2d}$$

Thus the energy transfer is of primary concern here. More convenient variables for treatment of these equations are the partial sums and differences of the intensities: $u_1 = I_2 + I_1$, $v_1 = I_2 - I_1$, $u_2 = I_4 + I_3$, and $v_2 = I_4 - I_3$. The new equations are given by

$$Iu_1' = 2gv_1v_2 + \gamma f_1^2, \tag{3a}$$

$$Iv_1' = 2gu_1v_2, \tag{3b}$$

$$Iu_2' = 2g(u_1u_2 + f_1f_2), \tag{3c}$$

$$Iv_2' = 2gu_1v_2, \tag{3d}$$

where now $I = u_1 + u_2$. The functions $f_1^2 = 4I_1I_2$ and $f_2^2 = 4I_3I_4$ obey similar equations,

$$If_1' = \gamma u_1 f_1, \tag{4a}$$

$$If_2' = 2g(u_1f_2 + f_1u_2), \tag{4b}$$

and this fact can be used to facilitate the solution of Eqs. (3). Equations (3b) and (4a) can be integrated in terms of v_2:

$$v_1 = v_2 + \Delta, \qquad f_1 = f_{1d}(v_2/v_{2d})^{\gamma/2g}, \tag{5}$$

where $\Delta = v_{1d} - v_{2d}$ is a constant evaluated at $z = d$, d being the thickness of the crystal. Knowledge of v_1 and f_1 permits the evaluation of $u_1 = (f_1^2 + v_1^2)^{1/2}$. In this manner three variables are expressed in terms of v_2. It remains to do the same for u_2 and f_2 and then to solve an equation for v_2. The complications are that all these variables are coupled and that they obey boundary conditions at different points.

A convenient way to resolve these problems is to introduce a new variable w by the definitions

$$u_2 = v_2 \cosh w, \qquad f_2 = v_2 \sinh w \tag{6}$$

and then to rescale all variables with respect to v_{2d}, i.e., to define $u = u_1/v_{2d}$, $f = f_1/v_{2d}$, and $v = v_2/v_{2d}$. The equations to be solved become

$$iv' = 2guv, \qquad iw' = 2gf, \tag{7}$$

where now $i = u + v \cosh w$, $u(v) = [(v + \delta)^2 + a^2v^b]^{1/2}$, and $f(v) = av^{b/2}$. The parameters $\delta = \Delta/v_{2d}$ and $a = f_{1d}/v_{2d}$, as will be seen below, are of special importance in our solution procedure. Here $b = \gamma/g$.

The system of Eqs. (7), apart from being integrable, has another nice property: it presents an initial-value problem. The values of both unknown variables are known on the $z = d$ face of the crystal: $v_d = 1$, $w_d = 0$. In this manner the boundary-value nature of the problem is transferred to the parameter space.

The solution of the system of Eqs. (7) is given in quadratures:

$$\ln[v(z)] + \int_1^v \frac{\cosh[w(x)]}{[(x + \delta)^2 + a^2x^b]^{1/2}}\,dx = 2g(z - d), \tag{8a}$$

$$w(v) = \int_1^v \frac{ax^{b/2-1}}{[(x + \delta)^2 + a^2x^b]^{1/2}}\,dx, \tag{8b}$$

but the integrals indicated cannot be evaluated in closed form for arbitrary b. With a good table of integrals many special cases ($b = 0, 1, 2, \ldots$) can be written down explicitly. Furthermore, numerical evaluation or tabulation of these integrals entails little difficulty. Even less troublesome numerically is to integrate Eqs. (7) directly on a computer as an initial-value problem. In any case there remains the problem of boundary values.

Let us denote the given values of intensities by $I_{10} = C_1$ and $I_{40} = C_4$ on the $z = 0$ face of the crystal and by $I_{2d} = C_2$ and $I_{3d} = 0$ on the $z = d$ face. The parameters a and δ are related to these by

$$a = 2(C_2I_{1d})^{1/2}/I_{4d}, \qquad \delta = (C_2 - I_{1d})/I_{4d} - 1, \tag{9}$$

where I_{1d} and $I_{4d} = v_{2d}$ are the missing boundary values at

$z = d$. The same parameters can also be related to the missing values I_{20} and I_{30} (or, equivalently, v_0 and w_0) at $z = 0$:

$$a^2 = 4C_1C_2x\frac{x(C_1 + C_2) + v_0 - 1}{C_1 + C_2v_0{}^b},$$
$$\delta = \frac{x(C_2{}^2v_0{}^b - C_1{}^2) - C_1v_0 - C_2v_0{}^b}{C_1 + C_2v_0{}^b}, \tag{10}$$

where $x = v_0(\cosh w_0 + 1)/2C_4$, which is also the inverse of v_{2d}.

The problem of boundary values is that a and δ are given in terms of v_0 and w_0, and these can be evaluated only after the correct values of a and δ are supplied to Eqs. (7) or (8). Such problems, however, are conveniently addressed by iteration procedures. Starting with some arbitrary initial values a_0 and δ_0, one substitutes these into Eqs. (7) or (8), integrates the equations, and finds the values of v_0 and w_0. From these the new values of a_1 and δ_1 are calculated, and the procedure is repeated until the desired accuracy is achieved. In this manner an iterative map in the plane is defined, and the procedure actually presents an evaluation of the fixed points of the map. It is our experience that this procedure converges rapidly and provides more accurate and stable solutions than standard methods for boundary-value problems, such as the shooting or relaxation algorithm. In addition, this procedure is also well suited for multistable situations, where other methods often fail.

There are four relevant control parameters in the problem: the wave mixing coefficients g and γ (actually gd and γd, but we keep $d = 1$ throughout) and the boundary values C_2 and C_4 (the other pump is used as the intensity unit, and C_1 is fixed to be 1). The most important parameter is the coupling coefficient g. In general, we found that the procedure is stable for negative g and arbitrary values of the other parameters. For positive g the method is stable up to approximately $g \approx 2$, and then it loses stability. In the remainder of this section we display some of the stable solutions. Unstable solutions and chaos are presented in Section 3.

The intensities are given in terms of the functions v and w:

$$I_1 = I_{4d}[u(v) - (v + \delta)]/2, \qquad I_2 = I_{4d}[u(v) + (v + \delta)]/2, \tag{11a}$$

$$I_3 = I_{4d}v(\cosh w - 1)/2, \qquad I_4 = I_{4d}v(\cosh w + 1)/2, \tag{11b}$$

where $u(v)$ is given above and I_{4d} is the inverse of x appearing in Eqs. (10). The intensity reflectivity of the crystal is given by

$$R = (\cosh w_0 - 1)/(\cosh w_0 + 1). \tag{12}$$

It is seen that the reflectivity is bounded by 1, as it should be in this case of equal-strength multigrating operation.[10]

Another interesting consequence of equal-strength multigrating operation is that it prevents double phase conjugation. Double phase conjugation (DPC) is the wave mixing process in which there are only two beams (A_4 and A_2) incident upon the crystal, but there is a generation of the conjugate beams in both propagation arms. As such, DPC is the property of transmission gratings, since these are the only gratings that can cause coherent energy transfer from beam A_2 into the conjugate of beam A_4, and

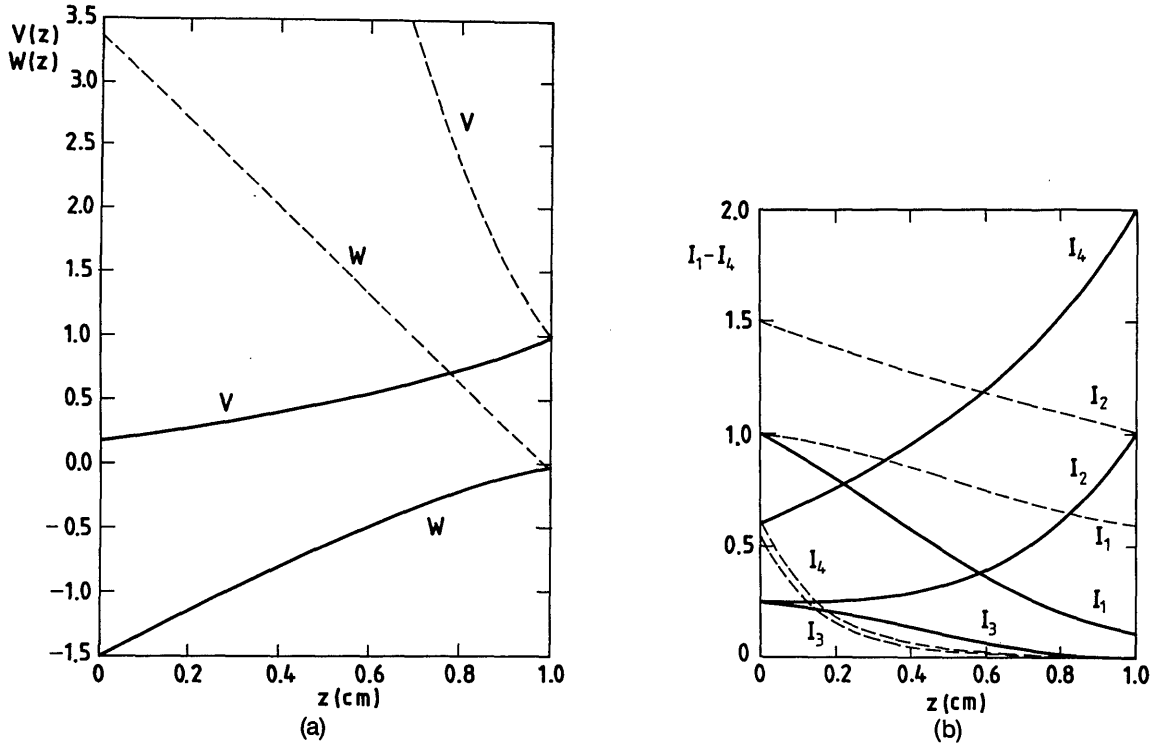

Fig. 1. (a) Functions $v(z)$ and $w(z)$ needed for specification of the intensities for parameters $g = 2$ (solid curves) and $g = -2$ (dashed curves). The other parameters are $\gamma = -1$, $C_2 = 1$, and $C_4 = 0.6$ (in units of the first pump intensity). (b) Corresponding intensities. It is seen that negative g attains higher reflectivity.

vice versa. DPC is not possible with reflective gratings. Moreover, it is not possible even in the case of equal-strength multiple gratings. This is evident if one inspects Eqs. (9) and (10) and the initial wave equations. It is seen that the condition $C_1 = 0$ implies that $a = 0$ and consequently $f = 0$. This means that $I_1 = 0$ everywhere, and there is no DPC.

Figure 1 depicts the functions $v(z)$ and $w(z)$ for $\gamma = -1$ and $g = \pm 2$ (in units of inverse centimeters) and the corresponding intensities $I_1 - I_4$. The behavior of v and w as functions of z is simple (hence the choice of these variables). v is always positive and is an exponentiallike function; it varies between 0 and 1 for positive g and is larger than 1 for negative g. w is more like a logarithmic function; it is negative for positive g and positive for negative g. For $g = 0$, v and w are constant (1 and 0, respectively), indicating that there is no phase conjugation (I_4 remains constant and $I_3 = 0$). In this case I_1 and I_2 experience two-wave mixing through the γ term. In general, the influence of the parameter γ on phase conjugation is not much pronounced.

Functions v and w are monotonic and, for reasonable values of g, could be easily linearized. We will not go into linearization here; however, we present an interesting case that is almost entirely linear but the tiny nonlinearity of which is essential for the explanation of the behavior of intensities. This is the case of $\gamma = 0$ and large and positive g.

As we mentioned above, large and positive g leads to instabilities in the system. Increasing g causes the system to become multivalued, chaotic, or even unphysical (with negative intensities). As far as we could establish, there is only one exception to this behavior, and that is the case when $\gamma = 0$ and when boundary conditions obey a certain relation. That is, if for arbitrary pumps $C_1 < C_2$ the initial signal is chosen as

$$C_4 = C_1(C_2 - C_1)/(C_2 + C_1), \tag{13}$$

then for arbitrarily strong g the map in the a–δ plane falls rapidly onto a fixed point:

$$a = 2C_1C_2/(C_2^2 - C_1^2), \qquad \delta = 0, \tag{14}$$

causing the appearance of a unique solution. An example of such behavior is shown in Fig. 2. It should also be noted that in this case the power flux to the left is balanced by the power flux to the right, i.e., $I_1 + I_4 = I_2 + I_3$. Furthermore, these P1 solutions are submerged into a sea of unstable solutions. If the prescribed boundary values are missed even slightly, the system goes to chaos or becomes unphysical. This situation is displayed in Fig. 3, where the first return map (a_n, a_{n+1}) is shown for $g = 24$, $C_2 = 6$, and $C_4 = 0.7$. Two chaotic segments in the form of a parabola are visible, signifying that this is a strongly dissipative case that can be described by a one-dimensional map. A fuller account of the instabilities arising in the system is provided in Section 3.

3. INSTABILITIES

Two interesting questions to be asked are whether the map can become unstable and what happens when it does become unstable. In other words, in addition to the fixed points of the map $(a_n, \delta_n) \rightarrow (a_{n+1}, \delta_{n+1})$, one may be interested in the fixed points of the arbitrary composition power of the same map. Such fixed points describe periodic orbits and may reveal the nature of the transition to chaos if there is one. As we mentioned in Section 2, the

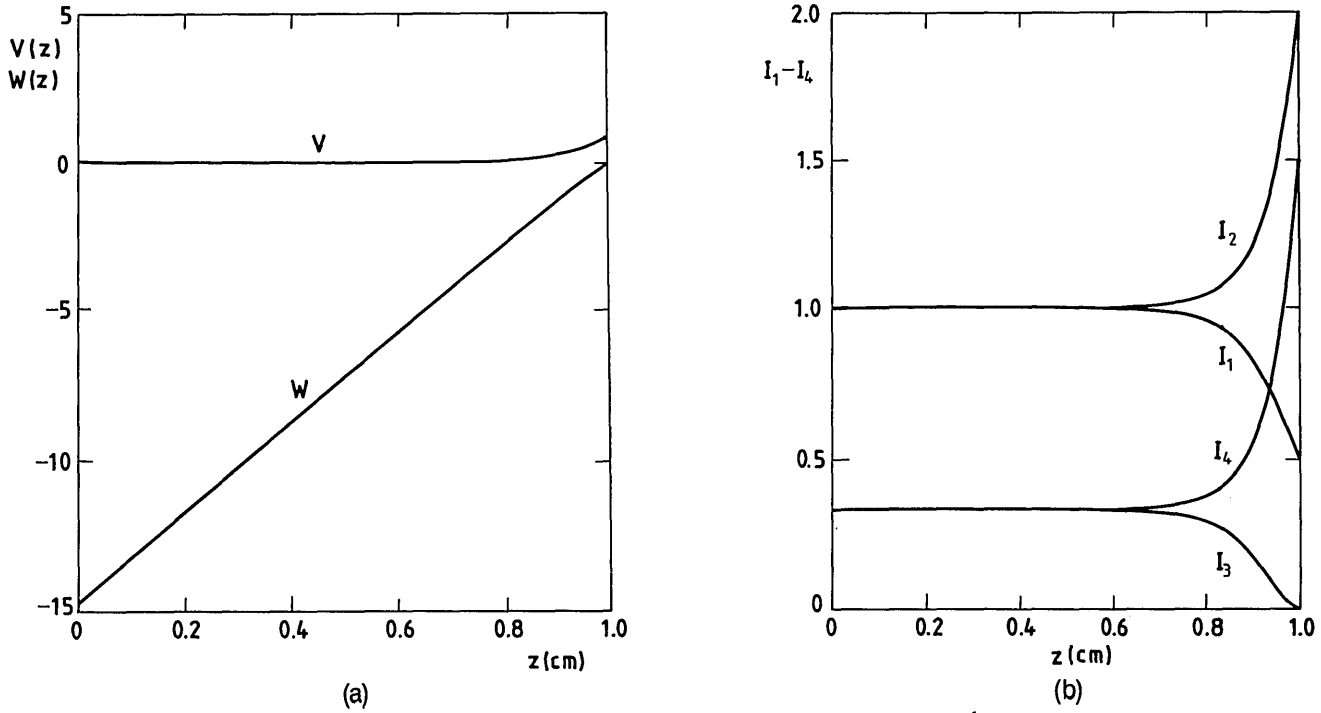

Fig. 2. (a) Functions $v(z)$ and $w(z)$ for the case $\gamma = 0$ and strong g coupling. Here $g = 10$ cm^{-1}, while the boundary conditions are $C_2 = 2$ and $C_4 = 1/3$. This choice leads to a unique fixed point ($a = 4/3$, $\delta = 0$) and an almost linear appearance of v and w. Note that v nearly equals 0, while the slope of w, given by $g(1 + C_1/C_2)$, equals 15. (b) Corresponding intensities. The slight nonlinearity visible in v and w causes an extremely large change in the intensities.

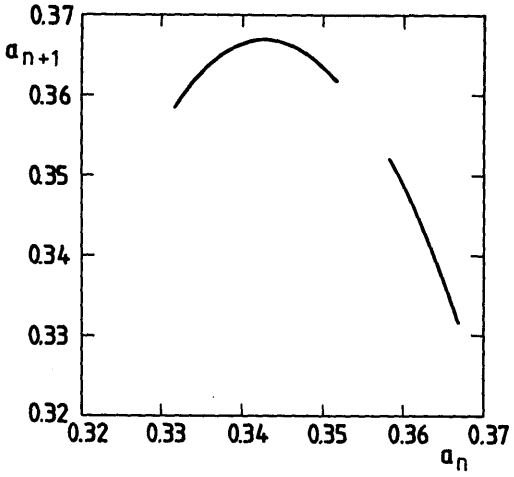

Fig. 3. First return map in a_n iterations for $g = 24$ cm^{-1}, $\gamma = 0$, $C_2 = 6$, and $C_4 = 0.7$. According to Eq. (13), for a unique strong-coupling solution, C_4 is supposed to be $5/7 \approx 0.7143$, and this small difference forces the appearance of (one-dimensional) chaos in a_n, while δ_n rapidly goes to 0.

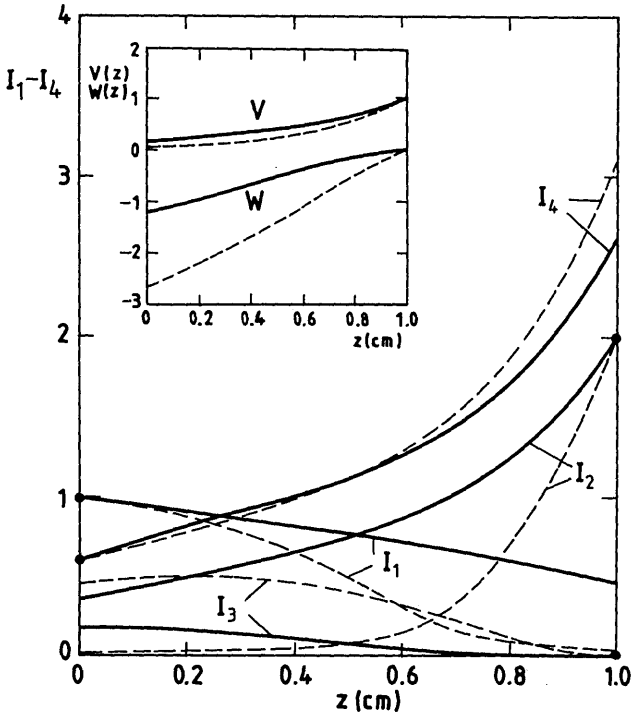

Fig. 4. Bistable P2 solution for $g = 2.89$, $\gamma = 1.5$, $C_2 = 2$, and $C_4 = 0.6$. On consecutive iterations the system jumps back and forth from the high-reflectivity, strong-depletion state (dashed curves) to the low-reflectivity, weak-depletion state (solid curves). The inset shows the corresponding v and w functions.

procedure is stable for $g < 2$ approximately. For $g > 2$, sooner or later it becomes unstable. The point where it actually becomes unstable, as well as the form of instabilities and their dynamics, depends strongly on the other parameters. We will follow here in some detail the dynamics of the system when g and γ are varied.

The most common instability observed is the P2 periodic motion. In that case, on consecutive iterations the system jumps back and forth from a high pump-depletion state to a low depletion state. Consequently, the reflectivity of the crystal blinks from a high value to a low value indefinitely. This solution is shown in Fig. 4. As a next complication, a P2 solution can coexist with a P1 solution. Which solution is reached depends on the initial conditions. A typical outlook of the domains of attraction in the α–δ plane is given in Fig. 5.

Other instabilities observed include quasi-periodic motion and a period-doubling route to chaos. The situation is presented by a phase diagram in Fig. 6. It is seen that, for this set of boundary values ($C_2 = 3, C_4 = 0.6$), chaos can be reached only in a band that separates P2 solutions from the unphysical solutions. Unphysical solutions in this context mean the solutions with negative a^2. Negative a^2 leads to the solutions with negative intensities, and the basic premises of the model then fail. There is no generation of the PC beam under these conditions. Such solutions must be discarded. It is an open question whether some of the other multistable solutions may also be discarded owing to some other physical constraint not so

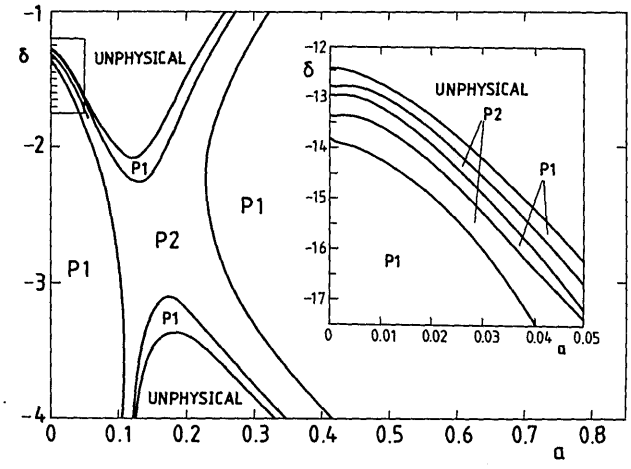

Fig. 5. Domains of attraction for the coexisting P1 and P2 states for driving parameters $g = 3.53$ and $\gamma = -0.2$, and boundary conditions $C_2 = 3$ and $C_4 = 0.6$. As $\alpha \to 0$, the domains start to intermingle, creating a fractal boundary. The inset depicts in more detail the interweaving P1 and P2 domains close to $\alpha = 0$.

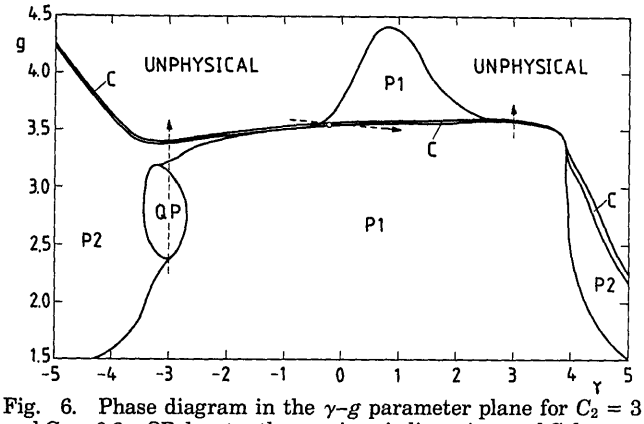

Fig. 6. Phase diagram in the γ–g parameter plane for $C_2 = 3$ and $C_4 = 0.6$. QP denotes the quasi-periodic region, and C denotes the chaotic band in which period doubling to chaos takes place. The region where a^2 becomes negative is labeled UNPHYSICAL. The chaotic band in the middle of the figure cuts across the P1 region, creating a domain where P1 and P2 solutions, or P1 and P4 solutions, or P1 and chaotic solutions can coexist. Which attractor is reached depends on the domains of attraction. The small circle near $\gamma = 0$ denotes the P1 and P2 coexistence point from Fig. 5. The dashed arrows denote directions of codimension 1 bifurcation diagrams presented in Figs. 11, 13, and 16.

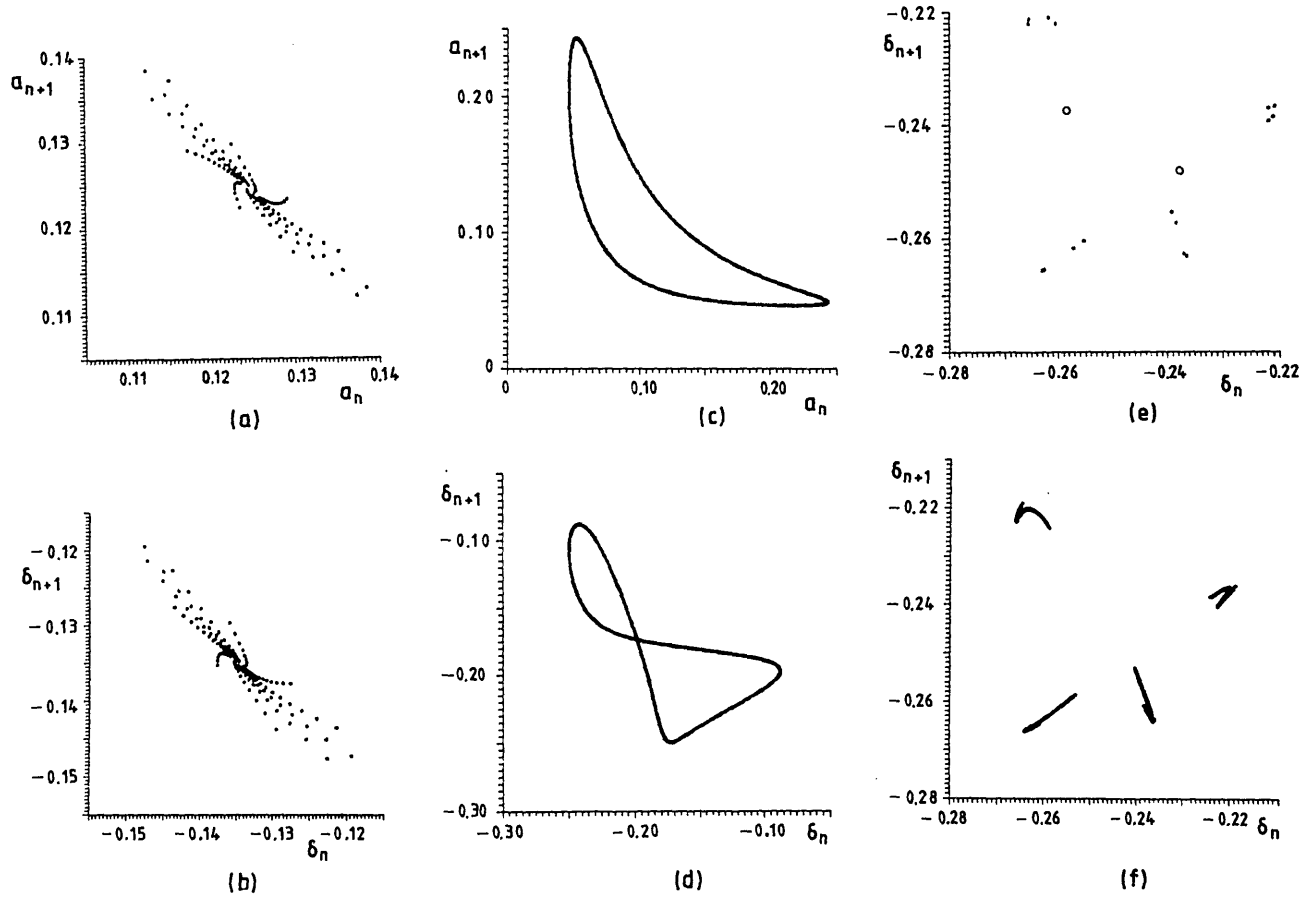

Fig. 7. Development of instabilities for $\gamma = -3$, $C_2 = 3$, and $C_4 = 0.6$ as g is varied. (a) and (b) Represent falling onto a limit cycle for $g = 2.3$, (c) and (d) exemplify motion on a torus at $g = 2.9$, and (e) is the beginning of a period-doubling cascade. The small filled circles stand for period 16 at $g = 3.3865$, and the open circles represent the period-2 cycle. (f) Four-piece strange attractor that develops for $g = 3.3869$.

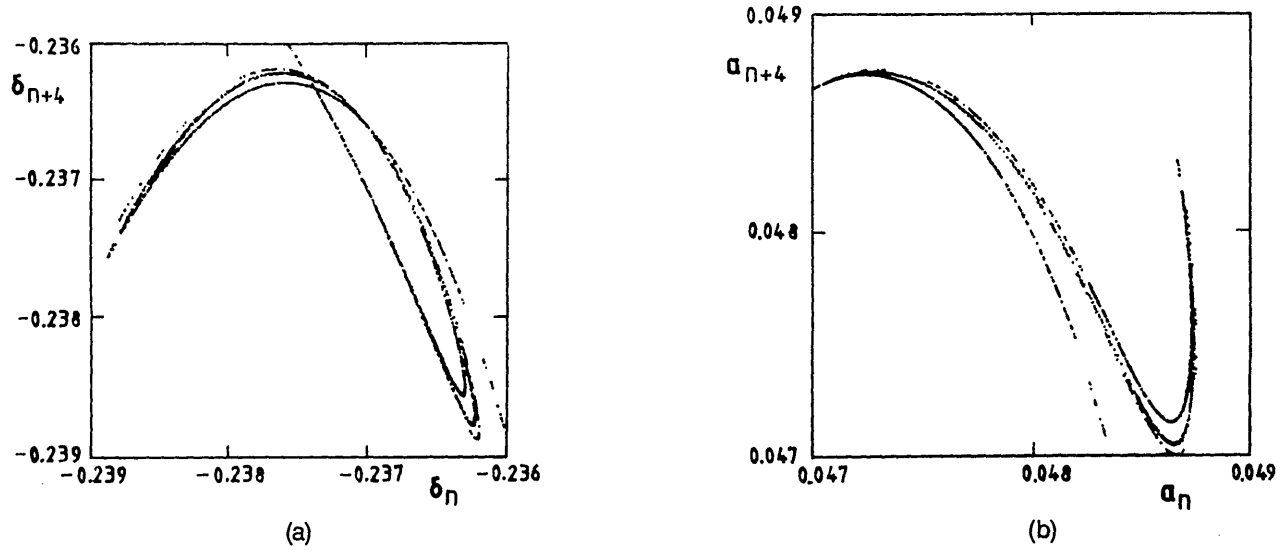

Fig. 8. Closeup of one of the four pieces of the attractor from Fig. 7(f) for (a) δ_n and (b) a_n sequences. Its fractal structure is evident.

readily apparent. In what follows we describe what happens with the system for some special cases from Fig. 6.

Figure 7 depicts the development of instabilities as g is varied for $\gamma = -3$. This case corresponds to the dashed line at the left of Fig. 6. Figures 7(a) and 7(b) show spiraling into a fixed point (limit cycle) in the Poincaré sections (return maps) of a and δ, while Figs. 7(c) and 7(d) display motion on a torus after a Hopf bifurcation has occurred in the system. With a further increase in g, invariant circles dissolve (collapse) back onto a fixed point in the a–δ plane, which then starts to bifurcate. Figure 7(e) depicts a period-16 cycle at $g = 3.3865$, and Fig. 7(f) illustrates a four-piece strange attractor that develops at $g = 3.3869$. To ascertain that the visible pieces are not one-dimensional

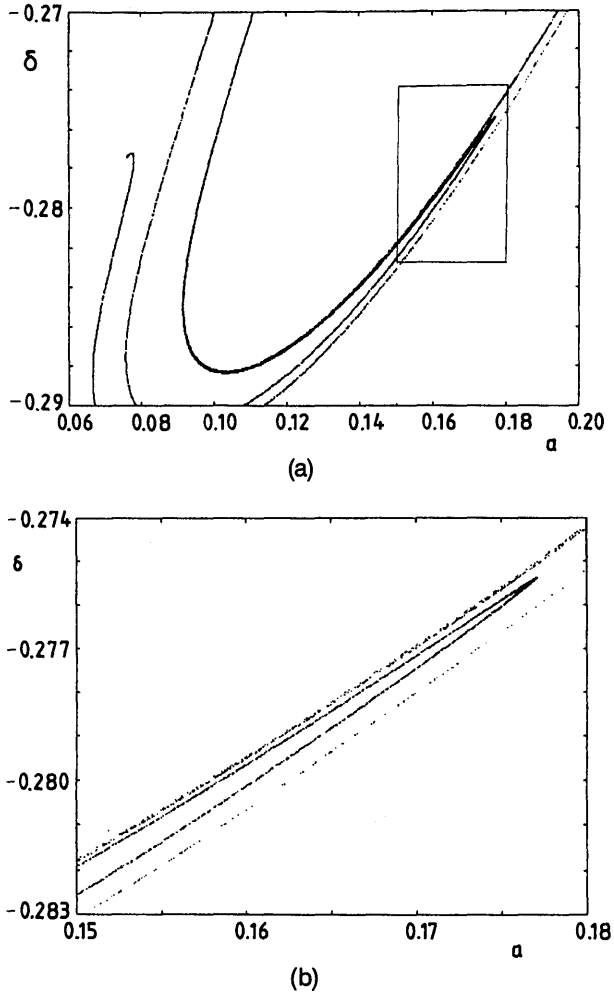

Fig. 9. Strange attractor in the plane of α–δ parameters. The inset in (a) is enlarged in (b) in order to demonstrate the fractal structure of the set.

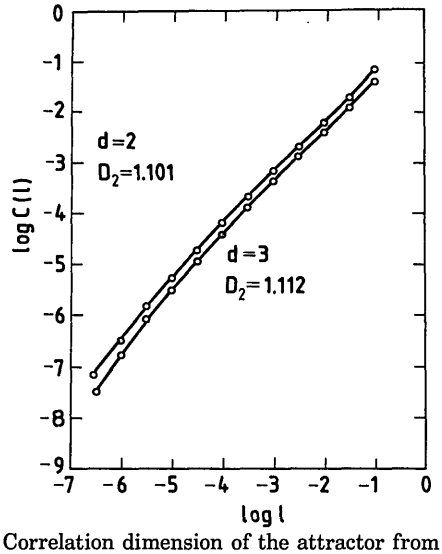

Fig. 10. Correlation dimension of the attractor from Fig. 9, obtained from embedding of the attractor in two-dimensional and three-dimensional Euclidean space.

segments in the plane, in Fig. 8 we provide a closer look at one of the pieces. The fractal structure of these sets is apparent.

A further increase in the parameter brings different pieces of the attractor together, and a one-piece strange attractor is formed. However, owing to the implicit and noninvertible nature of the map, it is difficult to draw stable and unstable manifolds of different fixed points. Figure 9 shows the attractor in the α–δ phase plane for

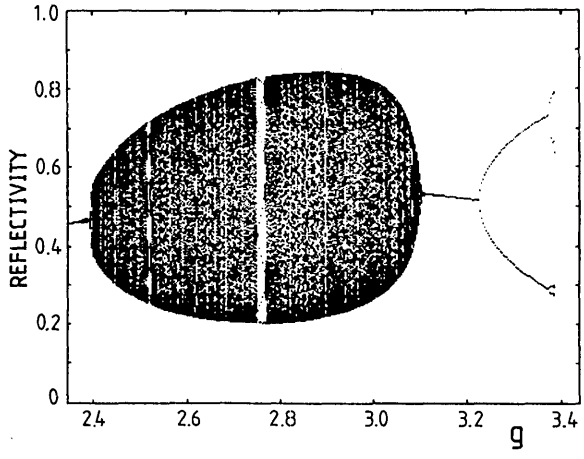

Fig. 11. Same development as in Fig. 7 but viewed as a bifurcation diagram of the intensity reflectivity.

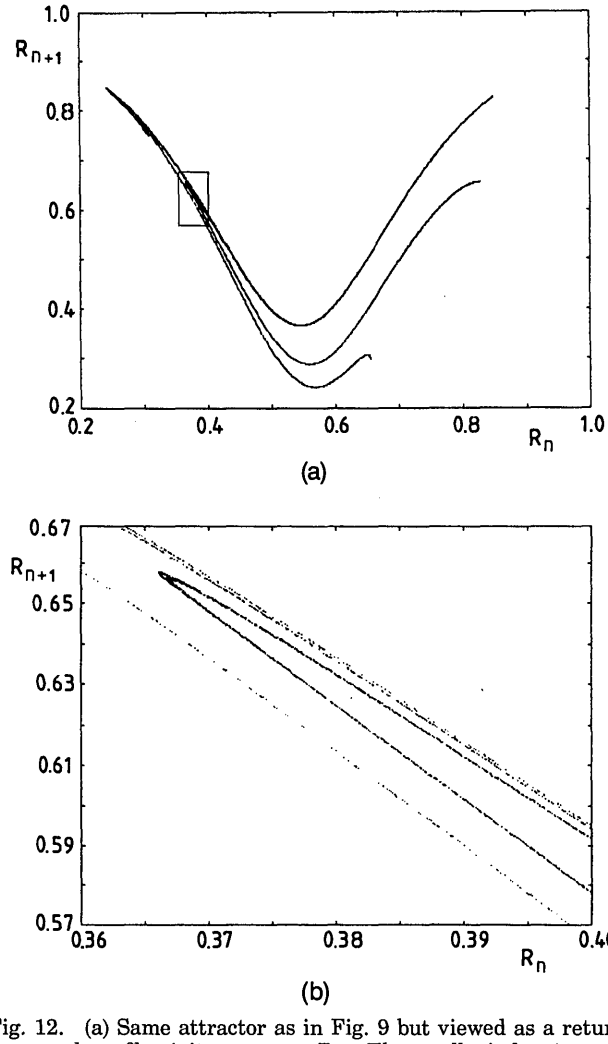

Fig. 12. (a) Same attractor as in Fig. 9 but viewed as a return map on the reflectivity sequence R_n. The small window (opened at approximately the same place as in Fig. 9) is enlarged in (b).

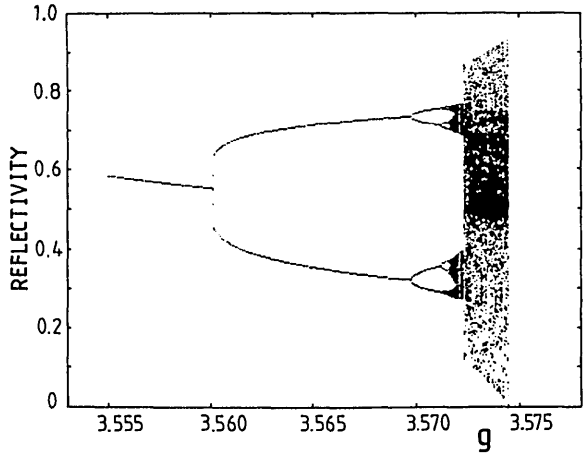

Fig. 13. Bifurcation diagram for positive γ ($\gamma = 3$). No quasi-periodic behavior is visible.

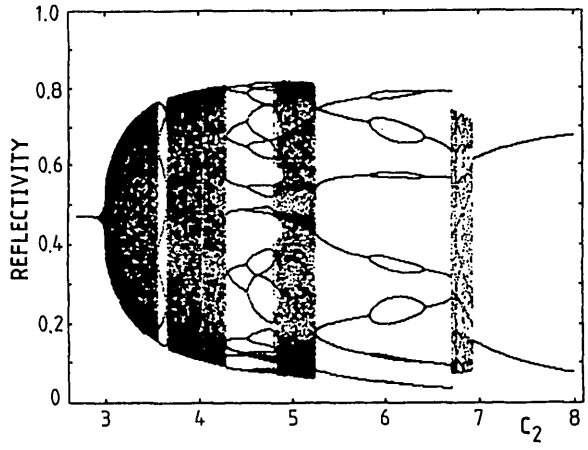

Fig. 14. Quasi-periodic instability of the intensity reflectivity of the crystal as a function of the pump intensity C_2 for $\gamma = -3$ and $g = 2.4$.

Figure 9 shows the attractor in the a–δ phase plane for $g = 3.505$, $\gamma = -1$, $C_2 = 3$, and $C_4 = 0.6$. We have measured its correlation dimension, using embedding techniques, and found it to be $D_2 \cong 1.1$ at this point in the parameter space (Fig. 10).

Figure 11 depicts the same development as Fig. 7 but in terms of the intensity reflectivity $R = I_{30}/C_4$ of the crystal. It makes little difference whether one looks at the chaos in the variables a and δ, or I_{1d} and I_{4d}, or I_{20} and I_{30}. The same qualitative behavior is observed. For example, the same strange attractor as in Fig. 9 is shown in Fig. 12, this time as a return map on the reflectivity. It is seen that roughly between $g \cong 2.35$ and $g \cong 3.12$ in Fig. 11 a quasi-periodic egg is formed, with many commensurate windows visible. The chaos, however, is not reached through quasi-periodicity, and at the end of the interval a unique, period-1 solution is recovered. This fixed point starts to bifurcate at approximately $g \cong 3.22$, and after a cascade of pitchfork bifurcations chaos is reached at $g \cong 3.39$. Thus, through a repeated loss of stability of the fixed points of various powers of the map, at a certain value of the wave coupling an aperiodic state is reached, where no stable reflectivity exists.

A different behavior is observed for positive γ. In Fig. 13 the development of the reflectivity is followed for $\gamma = 3$. This situation is shown by the small dashed line on the right of Fig. 6 above. Now no quasi-periodic egg appears, and the system proceeds to chaos through period doubling starting from $g \cong 3.56$. No structure (such as periodic windows) is visible in the chaotic region, and chaos actually terminates when the system enters an unphysical region of negative a^2.

Having a number of control parameters at our disposal, we can monitor the behavior of the system along different parameter axes. For example, Fig. 14 shows the behavior of the system as the input intensity of the second pump is varied while $\gamma = -3$ and $g = 2.4$ are kept fixed. This is the quasi-periodic region from Fig. 11. Here the quasi-periodic behavior is displayed in more detail. An interesting new detail is the appearance of primary bubbles in quasi-periodic windows. The system starts to bifurcate, but then, owing to some symmetry constraints (not explicitly apparent in our implicit map), it reverts to simple periodic behavior. Closer to the chaotic region (Fig. 15; $g = 3$, $\gamma = -0.5$), this behavior acquires the characteristics of merging bifurcations, or inverse period doublings.

A similar behavior is observed if the changes in the reflectivity are followed with the variations in γ (Fig. 16; $g = 3.53$, $C_2 = 3$). This situation is shown by the hori-

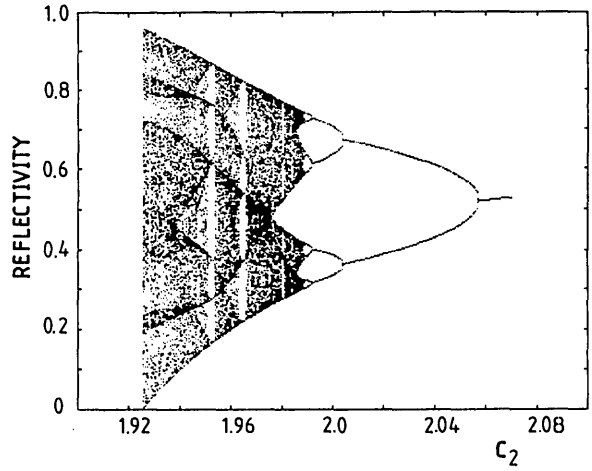

Fig. 15. Bifurcation diagram of the reflectivity with the pump intensity C_2 as the control parameter. The other parameters are $\gamma = -5$ and $g = 3$.

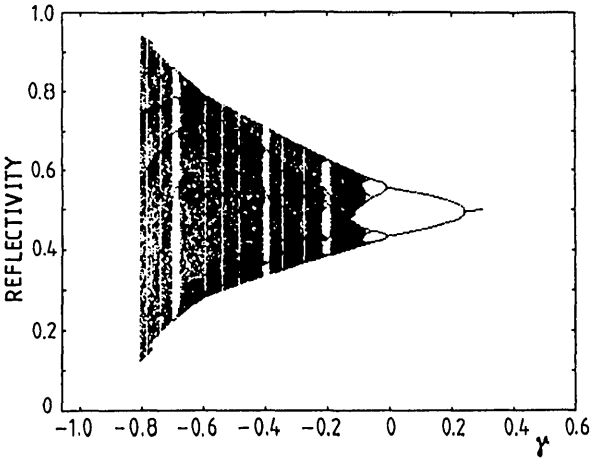

Fig. 16. Same as Fig. 15, but here the control parameter is γ. The other parameters are $g = 3.53$ and $C_2 = 3$.

zontal dashed line in Fig. 6. Generally, the phase diagram shows that the system is becoming more unstable as g is increasing and γ is decreasing (increasing) if it is negative (positive). Moreover, in the region of large g's (strong-coupling limit), a boundary is eventually approached, where unphysical solutions appear. Chaos is found in the band that separates periodic from unphysical solutions.

4. SUMMARY

In summary, we have presented a novel procedure for the treatment of stable and unstable outputs in optical phase conjugation. We analyze unstable, multivalued solutions that arise in standard 4WM geometry of photorefractive phase conjugation, using standard methods of nonlinear dynamics. Multigrating operation is assumed, and pump depletion is allowed. The initial boundary-value problem of slowly varying wave equations is transformed into an initial-value problem, which is solved in quadratures. In order to match boundary conditions, we construct an iterative map in the parameter space and analyze its stability. It is found that, as a function of the most important driving parameter g, the map is stable for $g < 0$ (which is the experimentally more preferred region), providing a unique solution to the original wave equations.

However, for $g > 0$ and increasing, invariably a region of instabilities is approached, where the map performs quasi-periodic motion, or becomes chaotic following a Feigenbaum period-doubling route to chaos. The chaotic region is rather narrow and featureless, and it ends in an unphysical region of negative intensities, where the model is inappropriate. The only exception to this behavior, as far as we could establish, is the set of solutions for $\gamma = 0$ with equal left and right fluxes. This set satisfies special boundary conditions and persists amid chaotic or unphysical solutions for arbitrarily large g.

It should be stressed at the end that the whole subject of chaos in OPC, or for that matter in any other optical system, is not firmly established if it arises in the analysis of steady-state equations. Looking at a long-time behavior in the systems in which temporal derivatives are neglected from the beginning could lead to spurious solutions or chaotic scenarios that are not observed in real life. This situation is similar to computational fluid dynamics, in which solving stationary potential equations leads sometimes to multiple solutions that are not found in Euler or Navier–Stokes equations.[11] In other words, the inclusion of temporal derivatives may lead to a completely different long-time behavior. One should exert great caution when dealing with multiple solutions in steady-state systems, since these may be an exclusive property of the model or approximation used or merely present a numerical instability. The possibly problematic physical content of instabilities and chaos obtained by steady-state analyses has received inadequate attention by researchers, yet such accounts are abundant in the literature. In our case we checked by an alternative method (brute-force shooting) that the instabilities belong to the wave equations at hand, but how real they are can be resolved only by experiment.

REFERENCES

1. See the May issue of J. Opt. Soc. Am. B **5** (1988).
2. R. A. Fisher, ed., *Optical Phase Conjugation* (Academic, New York, 1983).
3. See the August issue of J. Opt. Soc. Am. B **5** (1988) and the March issue of IEEE J. Quantum Electron. **25** (1989).
4. G. Valley and G. Dunning, Opt. Lett. **9,** 420–422 (1984); G. Reiner, M. R. Belić and P. Meystre, "Optical turbulence in phase conjugate resonators," J. Opt. Soc. Am. B **5,** 1193–1210 (1988).
5. P. Gunter, E. Voit, M. Z. Zha, and J. Albers, "Self-pulsation and optical chaos in self-pumped photorefractive $BaTiO_3$," Opt. Commun. **55,** 210–214 (1985).
6. D. J. Gauthier, D. Narum, and R. W. Boyd, "Observation of deterministic chaos in a phase conjugate mirror," Phys. Rev. Lett. **58,** 1640–1643 (1987).
7. For an introduction, see H. G. Schuster, *Deterministic Chaos* (Physikverlag, Weincheim, Germany, 1988).
8. W. Krolikowski, M. R. Belić, M. Cronin-Golomb, and A. Bledowski, "Chaos in photorefractive four-wave mixing with a single grating and a single interaction region," J. Opt. Soc. Am. B **7,** 1204–1209 (1990).
9. M. C. Golomb, B. Fisher, J. O. White, and A. Yariv, "Theory and applications of four-wave mixing in photorefractive media," IEEE J. Quantum Electron. **QE-20,** 12–30 (1984); "Amplified reflection, transmission, and self-oscillation in real-time holography," Opt. Lett. **6,** 519–521 (1981)
10. M. R. Belić, "Phase conjugation via multiple gratings in photorefractive crystals," Phys. Rev. A **37,** 1809–1812 (1988); W. Krolikowski and M. R. Belić, "Multigrating phase conjugation: exact results," Opt. Lett. **13,** 149–151 (1988).
11. M. D. Salas, "Foundations for the numerical solution of the Euler equations," in *Transonic Aerodynamics,* M. Habashi, ed. (Wiley, New York, 1985).